

# Determination of the transport scattering coefficient of red blood cells

A. T. Lovell<sup>a</sup>, J. C. Hebden<sup>b</sup>, J. C. Goldstone<sup>a</sup> and M. Cope<sup>b</sup>

<sup>a</sup> University College London Medical School, Division of Academic Anaesthesia, The Middlesex Hospital, Mortimer Street, London W1N 8AA, U.K.

<sup>b</sup> University College London, Department of Medical Physics and Bioengineering, 1<sup>st</sup> Floor, Shropshire House, 11-20 Capper Street, London WC1E 6JA, U.K.

## ABSTRACT

There are no reliable values for the transport scattering coefficient ( $\mu'_s$ ) of whole blood, particularly at the high hematocrits found in-vivo. Existing values are largely based on single scattering measurements of scattering cross-section and angular scattering. The accuracy of the single scattering method is limited by the accuracy with which the g-value can be measured, as it is near 0.99. Diffuse measurements, coupled to diffusion theory models, are normally hampered by the relatively high absorption coefficient of oxy-hemoglobin even in the near infrared. Blood was drawn from 9 healthy volunteers, heparinised, and the cells washed twice with phosphate buffered saline. Oxy-hemoglobin was converted to carbonmonoxide-hemoglobin, which has an absorption coefficient that is approximately 3% of that of oxy-hemoglobin in the near infrared region. Picosecond pulses of light were transmitted through an 80x60x20 mm cuvette and the resulting temporal point spread functions recorded with a streak camera. The data were fitted to a time-dependent diffusion model to derive values for  $\mu'_s$  and  $\mu_a$  which is now valid because of the low  $\mu_a$  of carboxy-hemoglobin. The effect of changing the hematocrit was determined by stepwise dilution of the washed red cells with further phosphate buffered saline. Mean values for  $\mu'_s$  and  $\mu_a$  at 802 nm were  $3.15 \pm 0.12 \text{ mm}^{-1}$  and  $0.0098 \pm 0.0004 \text{ mm}^{-1}$  respectively for the hematocrit in the normal range. The undiluted red cells showed a small negative wavelength dependence for  $\mu'_s$  over the range 740 to 860 nm with a slope of  $-0.0045 \pm 0.0011 \text{ mm}^{-1} \text{ nm}^{-1}$  which was highly significant ( $p=0.0001$ ). The negative wavelength dependence of  $\mu'_s$  is compatible with Mie theory predictions of scattering by large particles. A near linear relationship between  $\mu'_s$  versus hematocrit (H) was found in this study (up to  $H=0.45$ ) as opposed to the  $\mu'_s \propto H(1-H)$  or  $\mu'_s \propto H(1-H)(1.4-H)$  macroscopic scattering coefficient relationship of others.

**Keywords:** Red Blood Cells, Scattering Coefficient, Diffusion Model

## 1. INTRODUCTION

Although the Bouguer-Beer law has been shown to be applicable to hemoglobin solutions, even at high concentrations,<sup>1</sup> whole blood departs markedly from Beer's law.<sup>2-4</sup> In particular, the optical density of whole blood is proportional neither to the concentration of hemoglobin nor the thickness of the measuring cell. Kramer has reported that the optical density of whole blood is 7 to 20 times higher than the optical density of solutions with the same hemoglobin concentration.<sup>2</sup> The principle differences in optical density between solutions of hemoglobin and whole blood have been attributed to light scattering. Red blood cells constitute the primary absorbers and scatterers within whole blood<sup>5</sup> and as a result the optical properties of whole blood are largely determined by the optical properties of its constituent red cells.

In theory the transport of light through whole blood can be considered from four possible standpoints. Originally, determining the optical properties of tissue consisted of measuring the diffuse reflectance and transmission and mathematically modelling the results using a simple heuristic theory, the two flux approximation of Kubelka-Munk.<sup>6,7</sup> This assumes that the light field is isotropic at all times, which is generally untrue. It was soon realized that the heuristic parameters  $K$  and  $S$ , representing light absorption and scattering respectively, had to be replaced by parameters defined within a physical theory of light transport.

---

Further author information: (Send correspondence to A.T.L)  
A.T.L.: E-mail: a.lovell@ucl.ac.uk

The most widely applied equation in optical imaging is the radiative transfer equation (RTE). However, analytical solutions for the RTE have only been obtained for very simple cases, for example one-dimensional geometries such as planetary atmospheres. The diffusion approximation to the RTE, also known as the  $P_1$  approximation, can be solved exactly for simple geometries and in more complex cases it can be obtained numerically. Diffusion theory describes the optical properties of tissue in terms of two main parameters, an absorption coefficient  $\mu_a$  and a transport scattering coefficient  $\mu'_s$  where  $\mu'_s = \mu_s(1-g)$  and  $g$  is the mean cosine of the scattering angle and  $\mu_s$  is the scattering coefficient. It has been demonstrated that the diffusion approximation of the RTE is very useful for determining the optical properties of highly scattering media.<sup>8</sup>

The diffusion equation is more realistic than Kubelka-Munk theory in that it allows for linearly anisotropic radiation. Star<sup>9</sup> has shown that in thin tissue sections the  $P_1$  approximation is inadequate for describing light transport and that significant improvements can be made by using a  $P_3$  approximation.<sup>10</sup> However, this leads to a considerable increase in complexity especially with regard to the application of boundary conditions and dealing with collimated light sources and detectors where linear anisotropy can not be assumed. Reliable values for higher-order terms in the expansion of the scattering phase function are very difficult, if not impossible, to obtain experimentally for biological tissues although this is not the case for well defined optical phantoms.<sup>11</sup> This has led to a return to using  $P_1$  approximations for simple geometries. The limitations of the  $P_1$  approximation become significant when  $\mu_a \ll \mu_s(1-g)$ , ie  $\mu_a \ll \mu'_s$ . Unfortunately for whole blood at a physiological hematocrit  $\mu'_s$  is only slightly larger than  $\mu_a$  at near infrared wavelengths.<sup>12</sup>

To date most successes with describing the optical behaviour of whole blood have used Twersky's theory.<sup>13-15</sup> This multiple scattering theory assumes that the red cells can be treated as large tenuous absorbers and uses the Rayleigh-Gans approximation with a forward peaked scattering phase function. It partitions the attenuation into a Beer-Lambert extinction term and a scattering term that has a quadratic relationship to hematocrit. Loewinger was the first to point out that Twersky's theory might be applied to whole blood<sup>16</sup> and subsequent studies by Anderson<sup>3,4</sup> and Steinke<sup>17</sup> have confirmed its applicability when measurements are made in thin films. The effect of increased scattering by the red blood cell is most marked at high and low hematocrits. At low hematocrits, equal increases in hematocrit produce proportionally more scattering than at intermediate hematocrits, whereas at high hematocrits, the red cells start to abut each other and consequently less scattering occurs. Over the intermediate range of hematocrits the relationship between  $\mu_a \cdot l$  and attenuation becomes linear with a slope of approximately 3 rather than unity.<sup>17</sup> There are two possible explanations for a slope greater than unity in this linear region; it is known that increased scattering will directly lead to increased attenuation, and secondly that scattering will increase the pathlength that the light travels and therefore increase overall absorption.

Mie theory can be used to calculate the scattering cross section and angular distribution function. For low particle densities it is possible to scale this up to provide a scattering coefficient and  $g$  value. In theory, this relationship should break down at high particle densities. This theory has the advantages of providing an exact solution for Maxwell's equations and is valid for all sizes of spherical particles. Unfortunately in real life, red cells are biconcave disks rather than spheres. Nevertheless comparisons between experimental measurements and Mie theory have shown good agreement between reflected intensity<sup>18</sup> and scattering cross-sectional area<sup>5</sup> although the anisotropy of the red cells yields spuriously high values for the mean cosine of the scattering angle.<sup>5</sup> The reason for the overestimation of  $g$  by Mie theory is that randomly orientated non-spherical particles have a less forward peaked angular scattering function than their volume equivalent spheres.

Existing values for  $\mu'_s$  are largely based on single scattering measurements of scattering cross sectional area and angular scattering measurements.<sup>5</sup> The accuracy of this technique is limited by the accuracy with which  $g$  can be determined. Red blood cell suspensions are known to have a highly forward peaked scattering phase function<sup>5,19</sup> which results in  $g$  lying near to 0.99.<sup>12</sup> Conventional diffuse measurements coupled to diffusion theory models are hampered by the requirement that  $\mu_a \ll \mu'_s$ . Even in the near infrared region the absorption coefficient of oxy-hemoglobin is too high. At 800 nm  $\mu_a$  for whole blood with a hemoglobin concentration of 15 g·dl<sup>-1</sup> is 0.47 mm<sup>-1</sup> whilst the reported values for  $\mu'_s$  lie in the range 1.2 to 2.5 mm<sup>-1</sup>.<sup>12,20</sup> The absorption coefficient for carbonmonoxide-hemoglobin is only 5% that of oxy-hemoglobin at 800 nm<sup>21</sup> and we have exploited this fact in order to determine the transport coefficient for human red cells using a diffusive technique.

## 2. METHODS

### 2.1. Preparation of Carbonmonoxide-hemoglobin Red Cells

Following institutional Ethical Committee approval and with written informed consent we obtained 100 ml of venous blood from nine healthy volunteers. The blood was heparinised with 2500 iu heparin and centrifuged at 3000 rpm for ten minutes to precipitate the red blood cells. The plasma was discarded and replaced with an equal volume of isotonic phosphate buffered saline at pH 7.40 containing  $10 \text{ iu}\cdot\text{ml}^{-1}$  heparin. The cells were gently resuspended by rolling the centrifuge tubes and the resuspended cells washed twice more with further phosphate buffered saline.

The hemoglobin in the red cells was converted to carbonmonoxide-hemoglobin by bubbling 100% carbonmonoxide through the cell suspension whilst it was gently agitated for 20 minutes.

### 2.2. Determination of Optical Properties

Experimental data was aquired using the time-resolved system shown in Figure 1. Pulses of light of roughly picosecond duration are generated by a mode-locked Ti:sapphire laser (Spectra Physics, Tsunami) pumped by a diode-pumped

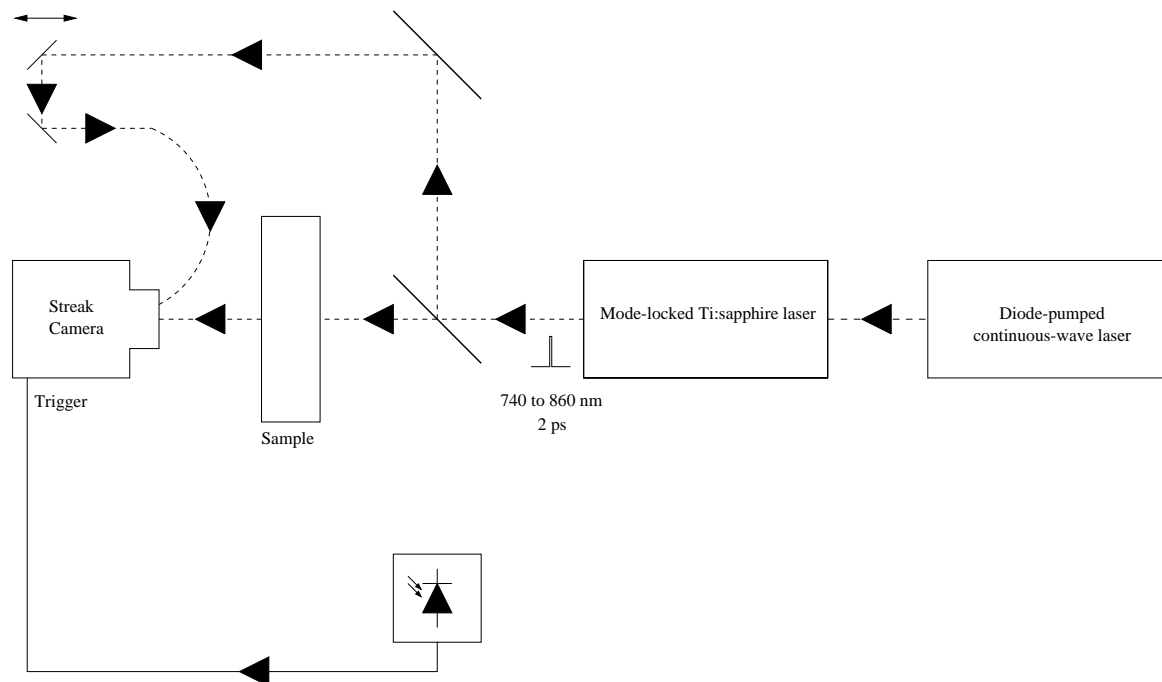


Figure 1. Experimental setup for measuring TPSFs

continuous wave laser (Spectra Physics, Millennium V). Wavelength is variable over a 740 nm to 860 nm range via an adjustable birefringent filter, and the power output is generally in the range 450 mW to 950 mW depending on wavelength. The blood sample was held in within a  $80 \times 60 \times 20$  mm cuvette, and light was delivered to the center of one of the largest faces via a single graded-index fiber. Light transmitted through the 20 mm thickness directly opposite the input fiber is relayed to the input slit of a streak camera (Hamamatsu Photonics, model C5680) via an optical fiber bundle, 2 mm in diameter. The streak images produced by the camera were averaged along the spacial direction to produce intensity versus time profiles (temporal point spread functions, or TPSFs) with a temporal resolution of about 20 ps. A reference pulse was also recorded directly from the laser which enables the absolute time delay produced by the sample to be determined. Transmitted light was integrated by the streak camera for between 5 and 50 seconds, depending on the opacity of the sample. In order to avoid problems due to sedimentation of the red cells, all measurements were made within two minutes of placing the cell suspension in the cuvette. Pre-processing involved performing several corrections for various sources of noise and system non-linearity. This included subtraction of the dark current produced by the CCD mounted on the rear of the streak camera, a shading correction to account for variation in gain across the face of the detector, and correction for the non-linear sweep of the streak camera along the temporal axis.<sup>22</sup>

Determination of the optical coefficients  $\mu_a$  and  $\mu'_s$  was achieved by comparing each experimental TPSF with an analytical model based on the Green function solution to the diffusion equation. Green functions are appropriate in the case where the source can be considered to be a delta function, and solutions have been published for a variety of simple homogenous geometries, for both time and frequency domain data.<sup>8,23</sup> The particular model used here is the time domain solution for an infinite slab geometry employing the so-called extrapolated boundary condition.<sup>24</sup> The model was incorporated into a least-squares fitting algorithm which derives the values of three parameters:  $\mu_a$ ,  $\mu'_s$ , and an arbitrary amplitude term. The corresponding uncertainty in each parameter is extracted from a co-variance matrix.

### 2.3. Experiment 1

The effect of changing the wavelength over the range 740 to 860 nm was assessed by tuning the Tsunami laser in approximately 8nm steps. The wavelength of the Tsunami laser was measured using a CCD spectrophotometer.<sup>25</sup> The relationship between wavelength and  $\mu'_s$  was determined by analysis of co-variance using a dummy variable to represent the nine subjects in order to correct for the multiple measurements made on each sample.<sup>26,27</sup>

### 2.4. Experiment 2

The effect of changing the hematocrit at a fixed wavelength of 802 nm was assessed by repeatedly diluting the red cell suspension with further isotonic phosphate buffered saline. At each stage 3 ml of the cell suspension was saved for determination of cell number, hematocrit and mean cell volume using a Coulter counter (Coulter Electronics Inc., Hialeah Fl). The relationship between the hematocrit and  $\mu'_s$  was determined by analysis of co-variance using a polynomial model.

### 2.5. Mie Theory Simulations

To compare our experimental results with Mie theory we used the BHMIE computer program of Borhen and Huffman.<sup>28</sup> For these calculations we assumed that the cells could be considered as spheres and calculated their mean diameter from the measured mean cell volume. The refractive index of the suspending phosphate buffered saline was taken as 1.33 and the refractive index of the red cells as 1.40.<sup>29</sup>

Statistical analysis was carried out using SAS 6.12 (SAS Institute, Cary NC) and results are quoted as mean  $\pm$  standard error.

## 3. RESULTS

All measurements were made at an ambient temperature of 26 to 28 °C. The mean values for  $\mu_a$  and  $\mu'_s$  at 802nm were  $0.0098 \pm 0.0004 \text{ mm}^{-1}$  and  $3.15 \pm 0.12 \text{ mm}^{-1}$  at a hemoglobin concentration of  $14.9 \pm 0.25 \text{ g}\cdot\text{dl}^{-1}$  and mean cell volume of  $90.3 \pm 0.77 \text{ fl}$ . The effects of changes in wavelength on  $\mu'_s$  are shown in Figure 2. There is considerable inter-subject variation in the values for  $\mu'_s$ , although a general decrease as a function of wavelength is evident for individual subjects. Analysis of co-variance demonstrated a very strong relationship between wavelength and  $\mu'_s$  with a corrected correlation coefficient of -0.765,  $p < 0.0001$  and a regression equation of  $\mu'_s = 4.14 - 0.0012\lambda$  where  $\lambda$  is the wavelength measured in nanometres.

The effects of changes in hematocrit on  $\mu'_s$  are shown in Figure 3. A least-squares analysis of the data using linear and higher-order polynomial models reveals a strong linear relationship described by the equation  $\mu'_s = 7.20 \times \text{hematocrit} + 0.180$ , and with a correlation coefficient of 0.984. Extrapolation of the relationship between the values for  $\mu'_s$  and hematocrit calculated by Mie theory shows that as expected, this passes through the origin, although the measured values for  $\mu'_s$  show a small positive offset. Analysis of co-variance of changes in mean cell volume during the stepwise dilution showed that there was a statistically highly significant reduction in mean cell volume during the reduction in hematocrit from 0.45 to 0.04,  $p < 0.0001$ . However, the mean reduction during the progressive dilution amounted to only 1.9 fl in total which is approaching the accuracy of the Coulter counter. If the red cells are considered to be spheres, this change in volume would equate to a reduction in red cell diameter of  $0.02 \mu\text{m}$ , a reduction of 0.72%.

The relationship between  $\mu'_s$  predicted by Mie theory and that derived from the TPSFs is shown in Figure 4. Analysis of co-variance confirmed that there was a very strong linear relationship between  $\mu'_s$  predicted by Mie theory and that measured with a corrected correlation coefficient of 0.983,  $p < 0.0001$ . The co-variance regression equation was  $\mu'_s(\text{TPSF}) = 1.10 \times \mu'_s(\text{Mie}) + 0.167$ . This shows that our measured values for  $\mu'_s$  exceed those predicted by

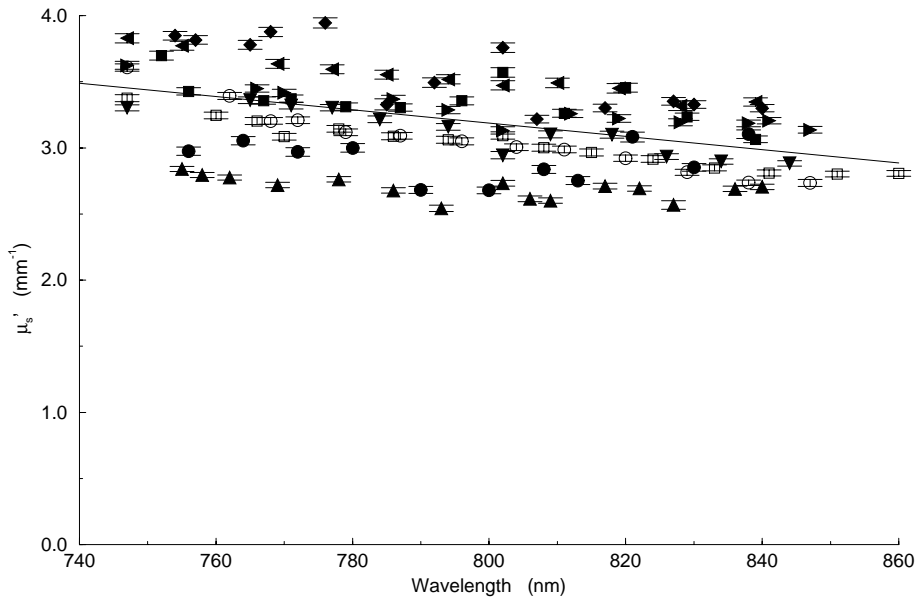


**Figure 2.** Effect on  $\mu'_s$  of changes in wavelength. Different symbols represent different subjects. The solid line represents the covariance regression line through the data.

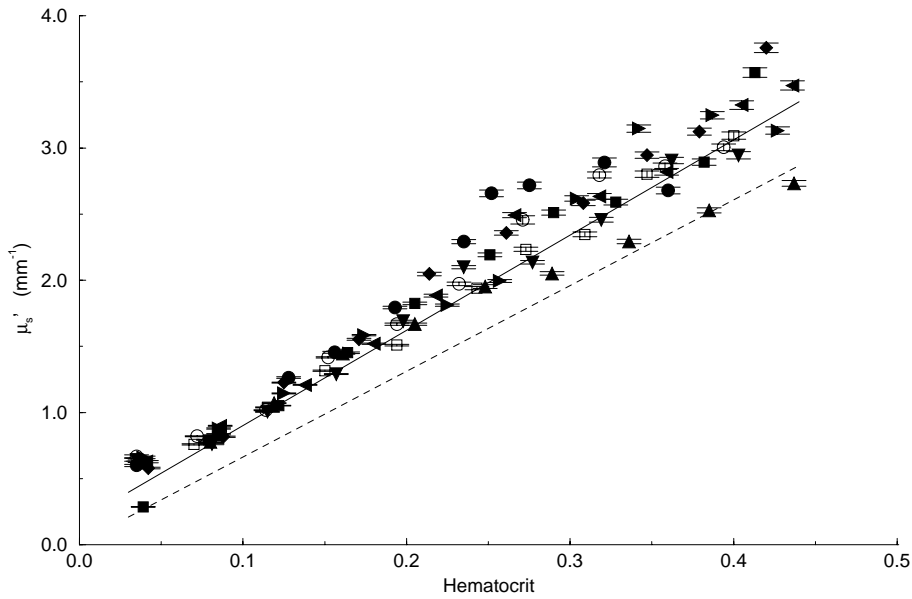


**Figure 3.** Effect on  $\mu'_s$  of changes in hematocrit at 802 nm. Different symbols represent different subjects. The solid line represents the covariance regression line through the data. The dashed line represents the co-variance regression through the Mie calculated values of  $\mu'_s$ .

Mie theory by approximately 10%. This may reflect either a systematic measurement error, or more likely be due to the marked anisotropy of human red cells which is a departure from the assumption of a spherical particle implicit in standard Mie theory.

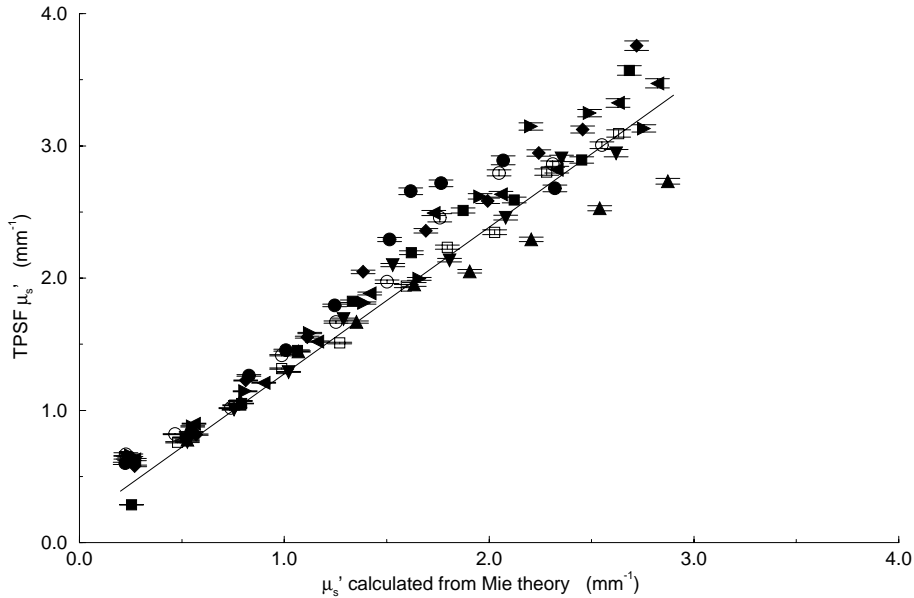


**Figure 4.** Relationship between  $\mu'_s$  predicted by Mie theory and  $\mu'_s$  derived from TPSF during changes in hematocrit at 802 nm. Different symbols represent different subjects. The solid line represents the covariance regression line through the data.

#### 4. DISCUSSION

Previous attempts at determining  $\mu'_s$  of red blood cells using a diffusion theory approach were hampered by the very high absorption coefficient of oxy-hemoglobin rendering the  $P_1$  approximation invalid. The conversion of the hemoglobin to carbonmonoxide-hemoglobin lowered  $\mu_a$  to only 0.3% that of  $\mu'_s$  thus rendering the  $P_1$  approximation valid. Our value for  $\mu_a$  for human red blood cells is 3.7% of that which has previously been reported<sup>12</sup> which is in excellent agreement with the absorption spectra data of Horecker showing that carbonmonoxide-hemoglobin has specific absorption coefficient of only 5% that of oxy-hemoglobin.<sup>21</sup> Our value for  $\mu'_s$  of  $3.15 \pm 0.12 \text{ mm}^{-1}$  at a hematocrit of  $0.407 \pm 0.008$  is considerably higher than previously reported values using a single scattering technique in thin films.<sup>12</sup> Nevertheless it lies within 10% of the value calculated by Mie theory.

We have found a clear negative wavelength dependence for  $\mu'_s$  that is compatible with the predictions of Mie theory. Additionally we have found that the relationship between hematocrit and  $\mu'_s$  is linear over the hematocrit range 0.04 to 0.45. This is precisely as predicted using the scattering cross section from Mie theory and the known red cell number but contradicts the previously reported curvilinear relationships of Twersky<sup>13-15</sup> and Loewinger.<sup>16</sup> However, none of these studies have made experimental observations that are capable of separating  $\mu_s$  and  $\mu_a$  at high hematocrits. The agreement between Mie theory was to within 10% over the range of hematocrits found in clinical practice.

#### 5. CONCLUSION

We have investigated the role of hematocrit and wavelength on the reduced scattering coefficient of human red blood cells. By converting the hemoglobin to carbonmonoxide-hemoglobin we were able to lower the value of  $\mu_a$  to enable the use of a diffusion approximation. At a hematocrit of  $0.407 \pm 0.008$  we found that  $\mu'_s$  was  $3.15 \pm 0.12 \text{ mm}^{-1}$ . There was a strong negative wavelength dependence of  $\mu'_s$  with a slope of  $-0.0045 \pm 0.0011 \text{ mm}^{-1} \text{ nm}^{-1}$  over the range 740 to 860 nm. Changes in hematocrit were linearly related to  $\mu'_s$  over the range 0.04 to 0.45. These data show good agreement with the changes predicted by Mie theory.

#### ACKNOWLEDGMENTS

This work was supported by a grant from the Wellcome Trust.

## REFERENCES

1. Drabkin DA, "The crystallographic and optical properties of the hemoglobin of man in comparison with those of other species," *J Biol Chem* **164**, pp. 703-23, 1946.
2. Kramer K, Elam JO, Saxton GA, Elam WN Jr, "Influence of oxygen saturation, ethryocyte concentration and optical depth upon the red and near- infrared light transmittance of whole blood," *Am J Physiol* **165**, pp. 229-46, 1951.
3. Anderson NM, Sekelj P, "Light-absorbing and scattering properties of non-haemolysed blood," *Phys Med Biol* **12**, pp. 173-84, 1967.
4. Anderson NM, Sekelj P, "Reflection and transmission of light by thin films of nonhaemolysed blood," *Phys Med Biol* **12**, pp. 185-92, 1967.
5. Steinke JM, Shepard AP, "Comparison of Mie theory and the light scattering of red blood cells," *Appl Opt* **27**, pp. 4027-33, 1988.
6. Kubelka P, Munk F, "Ein beitrag zur optik der farbanstriche," *Zeitschrift für technische Physik* **12**, pp. 593-601, 1931.
7. Kubelka P, "New contributions to the optics of intensely light- scattering materials. Part I," *J Opt Soc Am* **38**, pp. 448-57, 1948.
8. Patterson MS, Chance B, Wilson BC, "Time resolved reflectance and transmittance for the non-invasive measurement of tissue optical properties," *Appl Opt* **28**, pp. 2331-6, 1989.
9. Star WM, Marijnissen JPA, van Gemert MJC, "Light dosimetry in optical phantoms and in tissues: I Multiple flux and transport theory," *Phys Med Biol* **33**, pp. 437-54, 1988.
10. Star WM, "Comparing the P3-approximation with diffusion theory and with monte carlo calculations of light propagation in a slab geometry," in *Dosimetry of laser radiation in medicine and biology*, Müller GJ, Sliney DH, eds., SPIE Optical Engineering Press **IS 5**, pp. 146-54, 1989.
11. Star WM, "Light dosimetry *in vivo*," *Phys Med Biol* **42**, pp. 763-87, 1997.
12. Cheong W, Prah SA, Welch AJ, "A review of the optical properties of biological tissues," *IEEE Journal of Quantum Electronics* **26**, pp. 2166-85, 1990.
13. Twersky V, "Multiple scattering of waves and optical phenomena," *J Opt Soc Am* **52**, pp. 145-71, 1962.
14. Twersky V, "Absorption and multiple scattering by biological suspensions," *J Opt Soc Am* **60**, pp. 1084-93, 1970.
15. Twersky V, "Interface effects in multiple scattering by large, low-refracting, absorbing particles," *J Opt Soc Am* **60**, pp. 908-14, 1970.
16. Loewinger E, Gordon A, Weinreb A, Gross J, "Analysis of a micromethod for transmission oximetry of whole blood," *J Appl Physiol* **19**, pp. 1179-84, 1964.
17. Steinke JM, Shepherd AP, "Role of light scattering in whole blood oximetry," *IEEE Transactions on Biomedical Engineering* **BME33**, pp. 294- 301, 1986.
18. Pedersen GD, McCormick NJ, Reynolds LO, "Transport calculations for light scattering in blood," *Biophys J* **16**, pp. 199-207, 1976.
19. Frank KH, Kessler M, Applebaum K, Albrecht HP, Mauch ED, "Measurements of angular distributions of Rayleigh and Mie scattering events in biological models," *Phys Med Biol* **34**, pp. 1901-16, 1989.
20. Sardar DK, Levy LB, "Optical properties of whole blood," *Lasers in Medical Science* **13**, pp. 106-11, 1998.

21. Horecker BL, "The absorption spectra of hemoglobin and its derivatives in the visible and near infra-red regions," *J Biol Chem* **148**, pp. 173-83, 1943.
22. Hebden JC, Hall DJ, Delpy DT, "Spatial resolution performance of a time resolved optical imaging system using temporal extrapolation," *medical physics* **22**, pp. 201-9, 1995.
23. Arridge SR, Cope M, Delpy DT, "The theoretical basis for the determination of optical pathlengths in tissue: temporal and frequency analysis," *Phys Med Biol* **37**, pp. 1531-60, 1992.
24. Contini D, Martelli F, Zaccanti G, "Photon migration through a turbid slab described by a model based on diffusion approximation. 1. Theory," *Appl Opt* **36**, pp. 4587-99, 1997.
25. Cope M, Delpy DT, Wray S, Wyatt JS, Reynolds EOR, "A CCD spectrophotometer to quantitate the concentration of chromophores in living tissue utilising the absorption peak of water at 975 nm," *Adv Exp Med Biol* **248**, pp. 33-40, 1989.
26. Kleinbaum DG, Kupper LL, Muller KE, Nizam A, eds., *Applied regression analysis and multivariable methods*, 3rd ed., Duxbury Press, Pacific Grove, USA, 1998 .
27. Bland JM, Altman DG, "Calculating correlation coefficients with repeated observations: Part 1 - correlation within subjects," *Br Med J* **310**, pp. 446, 1995.
28. Borhen CF, Huffman DR, *Absorption and scattering of light by small particles*, John Wiley & Sons, New York, 1983 .
29. Bolin FP, Preuss LE, Taylor RC, Ference RJ, "Refractive index of some mammalian tissues using a fiber optical cladding method," *Appl Opt* **28**, pp. 2297-303, 1989.